ARPC5 Isoforms Drive Distinct Arp2/3-dependant Actin Remodeling Events in CD4 T Cells

Lopamudra Sadhu[1], Nikolaos Tsopoulidis[1, 3], Vibor Laketa[2], Michael Way[4, 5] and Oliver T. Fackler[1]

[1] Department of Infectious Diseases, Integrative Virology, University Hospital Heidelberg, Heidelberg, Germany

[2] Department of Infectious Diseases, Virology, University Hospital Heidelberg, Germany

[3] current address: Center for Regenerative Medicine, Mass General Hospital, Harvard Medical School, Boston, MA, USA

[4] Cellular Signaling and Cytoskeletal Function Laboratory, The Francis Crick Institute, London, UK

[5] Department of Infectious Disease, Imperial College, London, UK

Running title: ARPC5 isoform-specific actin dynamics in CD4 T cells

Corresponding author at:

Department of Infectious Diseases, Integrative Virology, University Hospital Heidelberg, Im Neuenheimer Feld 344, 69120 Heidelberg, Germany Phone: ++49-(0)6221-561322; Fax: ++49-(0)6221-565003; Email: oliver.fackler@med.uni-heidelberg.de

Summary

Nuclear actin polymerization is observed in an increasing number of biological processes including DNA replication stress [1-6] and T cell receptor (TCR) signaling in CD4 T cells [7]. TCR activation induces the formation of F-actin in the cytoplasm and the nucleus to strengthen contacts to antigen presenting cells and drive a gene expression program to shape humoral immune responses, respectively [7-11]. Interestingly, these two actin remodeling events are phenotypically different and appear to be mechanistically uncoupled from each other but both involve actin polymerization by the Arp2/3 complex. The Arp2/3-complex consists of 7 subunits where ARP3, ARPC1 and ARPC5 exist as two different isoforms in humans that can assemble in complexes with different properties [12-17]. Here we examined whether specific Arp2/3 subunit isoforms are responsible for distinct actin remodeling events in CD4 T cells. Transient silencing or knock out of individual subunit isoforms demonstrates that in response to TCR signaling, the ARPC5L isoform is involved in nuclear actin polymerization, while cytoplasmic actin dynamics selectively relies on ARPC5. In contrast, nuclear actin polymerization triggered by DNA replication stress in CD4 T cells required ARPC5 and was independent of ARPC5L. Moreover, nuclear Ca^{2+} transients, which are essential for TCR-induced nuclear actin polymerization, were dispensable for nuclear actin filament formation during DNA replication stress. Our results reveal that the selective involvement of ARPC5 isoforms governs the activity of Arp2/3 complex in distinct actin polymerization events and imply nuclear Ca^{2+} transients as selective trigger for ARPC5L-dependent nuclear actin polymerization.

Keywords: Nuclear F-actin, Arp2/3 complex, CD4 T cell activation, DNA replication stress

Results and discussion

To assess the involvement of Arp2/3 complex in cytoplasmic and nuclear actin dynamics, we performed *in vitro* high-speed confocal cell imaging of Jurkat CD4 T cells stably expressing a nuclear lifeact-GFP reporter (JNLA) after plating the cells on dishes coated with anti-CD3 and anti-CD28 antibodies [7] (Fig. 1A). In DMSO treated control cells, TCR engagement rapidly induced a transient burst of a nuclear F-actin (NFA) meshwork, which was followed by cell spreading and actin polymerization into a circumferential F-actin ring (AR) at the cell periphery (Fig. 1B-D, Suppl. Video 1). Pretreating the cells with the Arp2/3 inhibitor CK-869 prevented the formation of both NFA and AR with comparable efficacy (Figs.1B-D, Suppl. Video 2). Arp2/3 complex dependent actin polymerization in the nucleus and at the cell-cell contacts was also observed in the context of an immune synapse between JNLA cells with Staphylococcus enterotoxin E (SEE) superantigen loaded Raji B cells (Fig 1E-H, Suppl. Videos 3, 4). In line with our previous findings [7], these results establish that the Arp2/3-complex mediates similar, dynamically and phenotypically discernable, cytoplasmic and nuclear actin polymerization in CD4 T cells in response to T cell activation.

Nuclear but not cytoplasmic actin polymerization in response to T cell activation depends on nuclear Ca^{2+} transients and activation of nuclear ARP2. Both processes are thus regulated by distinct mechanisms and occur independently of another [7]. In search for the molecular basis for this differential regulation of Arp2/3 complex, we hypothesized that nuclear and cytoplasmic actin polymerization involves distinct Arp2/3-complex subunit isoforms [12-17]. Analyzing the mRNA and protein expression profile of Arp2/3 subunit isoforms in Jurkat CD4 T cells and primary human CD4 T cells revealed the ARPC1A and ARPC5 isoforms that were previously identified in mouse fibroblasts are also expressed in human CD4 T cells (Fig. 1I, Fig. S1). TCR stimulation in primary CD4 T cells increased mRNA levels of all subunits

and all subunits and isoforms were readily detected by western blotting for both, resting (R) and activated (A) CD4 T cells.

To assess the role of Arp2/3 subunit isoforms in these actin polymerization events, we transduced bulk JNLA cultures with isoform-specific shRNAs to reduce the expression of ARPC1A, ARPC1B, ARPC5 or ARPC5L (Fig. 2A). Unlike direct TCR stimulation, where Arp2/3-complexes are activated at the plasma membrane as well as in the nucleus, PMA/Ionomycin (P/I) increases intracellular Ca^{2+} and only triggers nuclear actin polymerization [7]. Selective silencing of ARPC1A, ARPC1B or ARPC5 did not significantly reduce the frequency of cells with NFA. In contrast, JNLA cells with reduced ARPC5L levels were significantly impaired in NFA formation in response to P/I (Figs. 2B, C). As with NFA, ARPC1A or ARPC1B were both able to support the formation of cytoplasmic AR after surface mediated TCR stimulation (Figs. 2D-E, see Figs. S2A for a lower magnification overview and Figs. S2B-D for quantification of cell morphologies). Importantly, ARPC5 but not ARPC5L was required for efficient cytoplasmic AR assembly. Also, upon surface mediated TCR stimulation of JNLA cells, ARPC5L mediated the formation of NFA (Figs. S2E, F).

Our observations pointed to a central role for ARPC5 and ARPC5L in the specificity of Arp2/3 driven cytoplasmic and nuclear actin polymerization in response to CD4 T cell activation. To confirm and/or extend our observations with transient silencing, we generated ARPC5 or ARPC5L knock out (KO) cell lines by CRISPR-Cas9 ribonucleoprotein transfection (Fig. 3). ARPC5 or ARPC5L were both virtually undetectable in the resulting bulk KO cultures (Fig. S3A). The levels of other Arp2/3 subunits remained largely unaffected with the exception of ARPC1B that was expressed to lower levels compared to the non-targeting control (NTC) (Figure S3A). The nucleofection and transduction procedures used to

generate and study these KO cells slightly reduced the overall efficiency of NFA formation in response to T cell activation. Nevertheless, T cell stimulation confirmed that ARPC5 is selectively required for cytoplasmic actin polymerization and is not substituted by the elevated levels of ARPC5L. In turn, ARPC5L is essential for NFA formation and dispensable for cytoplasmic actin polymerization (Fig. 3A-B, see mCherry controls). These effects were not due to off target effects as reintroduction of the respective mCherry tagged ARPC5 isoform in these KO cells reconstituted their ability to form NFA or ARs (Fig. 3A-B; S3B-C).

Actin polymerization at sites of TCR engagement is directly coupled to downstream signalling constituted by dynamic phosphorylation cascades occurring in induced signalling platforms referred to as microclusters [18-22]. Nuclear actin dynamics precedes cytoplasmic actin polymerization upon TCR stimulation but whether NFA formation affects microcluster formation or function is unclear. We therefore tested whether ARPC5 isoforms differently impact generation and composition of these microclusters. Disruption of cytoplasmic actin polymerization upon KO of ARPC5 significantly reduced the number of signalling microclusters as well as the amount of tyrosine phosphorylation (pTyr) or phosphor -SLP-76 (pSLP-76) within the microclusters (Fig. S4A-C and S4D-F). In contrast, loss of ARPC5L had no obvious effect on the formation and composition of TCR signaling induced microclusters. Together, these results revealed that in response to CD4 T cell activation, ARPC5 and ARPC5L selectively mediate actin polymerization at the plasma membrane including TCR proximal signaling or actin dynamics in the nucleus, respectively.

We next assessed whether the differential effect of ARPC5 and ARPC5L reflects their distinct cellular distribution. Since antibody staining did not allow to distinguish between the distribution of endogenous ARPC5 and ARPC5L, we examined the localization of transiently expressed the mCherry tagged isoforms that functionally rescued our KO cell lines. Both,

mCherry tagged ARPC5 and ARPC5L had a diffuse cytoplasmic distribution but were also detected in larger aggregates/punctae in the cytoplasm and the nucleus (Fig. 3C). Consistent with this, immunoblot analysis of nucleo-cytoplasmic fractionations reveals that endogenous ARPC5 and ARPC5L are both present in the nucleus, albeit at lower levels than the cytoplasm (Fig. S4G). This distribution of ARPC5 and ARPC5L was unaffected by the loss of expression of the other ARPC5 isoform. To better assess the localization of ARPC5.mCherry and ARPC5L.mCherry relative to the NFA network, we applied two-color super resolution STED microscopy on P/I-stimulated A301 CD4 T cells, which are best suited to visualize endogenous NFA meshworks in T cells and in which NFA formation depends on nuclear Arp2/3 complex induced by Ca^{2+} signaling [7]. Deconvolved and segmented STED images revealed a complex NFA meshwork (Fig. 3D). ARPC5.mCherry and ARPC5L.mCherry were both detected in discrete spots within the nucleus and approx. 10% of these spots co-localized with nuclear actin filaments, however, no significant difference was observed between both isoforms (9.9% for ARPC5, 13.2% for ARPC5L, see also Fig. S4H). The identity of the ARPC5 isoform involved therefore does not determine the ability of Arp2/3 complexes to associate with actin filaments in the nucleus.

We next sought to test whether the selective involvement of ARPC5L is a common principle for Arp2/3-dependent nuclear actin polymerization events. Arp2/3 also mediates nuclear actin polymerization in response to DNA replication stress induced by the DNA polymerase inhibitor Aphidicolin (APH) [4]. Similar to the results obtained by Lamm et al. (2020) in fibroblasts and epithelial cells, APH treatment of JNLA cells induced DNA replication stress as indicated by phosphorylation of the checkpoint kinase CHK-1 (Fig. S5A) and the formation of a NFA network that is maximal approx. at 90 min post treatment (Fig. 4D, see Fig. S5B for tracks of individual cells). This NFA meshwork appeared to consist of fewer but thicker F-actin bundles and to disassemble more slowly than when induced by TCR activation

(Fig. 4B, C). Next, ARPC5L and ARPC5 KO cells were stimulated in parallel by TCR engagement or APH. For TCR activation, this confirmed the requirement of ARPC5 for formation of actin ring (AR) and ARPC5L for the NFA network (Fig. S5C). In contrast, NFA formation in response to APH was indistinguishable to control cells in ARPC5L KO cells formed that (Figs 4B, C) but significantly impaired in ARPC5 KO cells. NFA induction by T cell activation or DNA replication stress is thus mediated by specific Arp2/3 complexes containing distinct ARPC5 subunit isoforms but nuclear localization of the actin polymerization event does not govern the involvement of the ARPC5 or ARPC5L isoforms. We therefore tested if this specificity for ARPC5 isoforms is provided by upstream signaling. NFA formation induced by T cell activation is mediated by nuclear calcium transients and can be inhibited by interfering with nuclear calmodulin by expressing a dominant negative version of calmodulin binding protein 4 (CAMBP4) [7, 23] (Fig. 4E, F). In contrast, dominant negative CAMBP4 did not affect NFA formation or CHK-1 phosphorylation upon APH treatment of JNLA cells (Fig. 4E-F and S5A). Similarly, pharmacological inhibitors of downstream effectors of calmodulin including Calmodulin-kinase kinase inhibitor STO609 as well as the Calmodulin-kinase II inhibitors KN93 and KN62 did not prevent NFA induction by APH (Fig. S5D). These results suggest nuclear Ca^{2+}-calmodulin acts as the selective trigger for ARPC5L-dependent nuclear actin polymerization.

A main finding of our study is that nuclear and cytoplasmic actin polymerization triggered by TCR engagement is specifically mediated by Arp2/3 complexes containing ARPC5L or ARPC5, respectively. The comparison of TCR signaling and APH-mediated induction of DNA replication stress revealed that nuclear actin polymerization events induced by these different stimuli are mediated by Arp2/3 complexes with distinct ARPC5 subunit preferences. Since Arp2/3 complexes containing both isoforms are present and operational in the nucleus, the selectivity for an ARPC5 isoform is not determined at the level of subcellular distribution.

Rather, the nature of the stimulus appears critical for the selective induction of actin polymerization by ARPC5 or ARPC5L containing Arp2/3 complexes (see schematic model in Fig. 4G) and our results suggest nuclear calcium-calmodulin signaling as specific trigger of ARPC5L containing complexes. It will be interesting to determine whether induction of ARPC5L-containing complexes by calcium-calmodulin can also occur in the cytoplasm. As described for N-Wasp [24-26], nucleation promoting factors (NPFs) that stimulate Arp2/3 can be activated by calcium-calmodulin. This suggests that ARPC5L containing complexes may contain specific NPFs that are subject to direct or indirect activation by calcium-calmodulin. In contrast, Arp2/3 complexes containing ARPC5 such as those involved in DNA replication stress trigger nuclear actin polymerization independently of calcium-calmodulin. It is tempting to speculate that the responsiveness to nuclear calcium transients by ARPC5L containing Arp2/3 complexes reflects the requirement for rapid conversion of an extracellular signal, e.g., to elicit a transcriptional response. In contrast, DNA replication stress provides a signal from within the nucleus without the need for a fast second messenger. Notably TCR signaling or DNA replication stress induce NFA networks of different filament morphology and dynamics. These architectural differences may translate into distinct functional roles of thin/dynamic filaments in transcriptional regulation following TCR engagement and thicker and more stable filaments that exert mechanical functions during DNA repair. The preference for distinct ARPC5 isoforms may adjust the activity of Arp2/3 complex to such divergent actin polymerization events. Defining the molecular basis of the selectivity of ARPC5 or ARPC5L-containing Arp2/3 complexes for their respective stimulus and how the architecture of NFA is tailored to specific functions will be an important goal of future studies.

208

209 ## Acknowledgments

210 We are grateful to Nadine Tibroni and Ina Ambiel for technical assistance and Kathrin Bajak
211 for help with manuscript preparation and submission. This project is supported by the
212 Deutsche Forschungsgemeinschaft (DFG, German Research Foundation) by project FA
213 378/20-1 to OTF. MW was supported by Cancer Research UK (FC001209), the UK Medical
214 Research Council (FC001209), and the Wellcome Trust (FC001209) funding at the Francis
215 Crick Institute as well as by the European Research Council (ERC) under the European
216 Union's Horizon 2020 research and innovation programme (grant agreement No 810207 to
217 MW). For the purpose of Open Access, the author has applied a CC BY public copyright
218 licence to any Author Accepted Manuscript version arising from this submission.

219

220

221 **Author contributions**

222 Conceptualization, O.T.F., N.T., Methodology, L.S., N.T., V.L.; Investigation, L.S., N.T.,
223 V.L.; Data analysis, L.S., N.T., V.L.; Writing – Original Draft, O.T.F., L.S.; Writing –
224 Review & Editing, O.T.F, M.W., L.S., N.T., V.L.; Funding Acquisition, O.T.F.; Resources,
225 M.W; Supervision, O.T.F

226

227

228 **Declaration of interest**

229 The authors declare no competing interests.

230

231

232

Figure Legends

Fig. 1. Arp2/3 complex mediated nuclear and plasma membrane actin polymerization in CD4 T cells. (A) Schematic representation of the experimental/live cell imaging set up as performed for figures B-D**.** (**B**) Jurkat CD4 T cells stably expressing nuclear lifeact-GFP (here on referred to as JNLA.GFP), pre-treated with either DMSO (solvent control) or CK869 for 30min, were put on TCR stimulatory GBDs and subjected to live-cell microscopy. Shown are representative still images from the spinning-disk confocal microscope from the time the cells fall on the coverslips until after contact with the stimulatory surface, with acquisition every 30s. Arrows indicate the nuclear F-actin (NFA) whereas arrowheads point to the F-actin at PM. Quantification of nuclear (**C:** nuclear actin filaments [NFA]) and plasma membrane (**D:** F-actin ring [AR]) polymerization are shown, respectively, upon contact with TCR stimulatory surface. Data points indicate mean values from three independent experiments where 40-60 cells were analyzed per condition in each experiment. Scale bar, 5µm. **(E)** Schematic representation of the experimental/live cell imaging set up as performed for F-H. (**F**) Shown are representative still images at indicated time points from live-cell visualization of nuclear and plasma membrane actin dynamics in JNLA.GFP cells treated as above with either DMSO or CK869 upon contact with SEE pulsed Raji B cells. Images were acquired every 70s for a total of 30min after adding the Raji B cells. Quantification of nuclear (**G**, NFA) and plasma membrane (**H**, AR) F-actin dynamics of JNLA.GFP cells upon contact with SEE pulsed Raji B cells are shown respectively. All data points indicate mean values from three independent experiments with at least 40 cells analyzed per condition per experiment. Statistical significance based on the calculation of mean ± SD from three independent experiments, using Welch's t-test were performed. *$P \leq 0.0332$, **$P \leq 0.0021$and *ns*: not significant. Scale bar, 7µm. **(I)** Expression of all the subunits of the Arp2/3 complex along with the isoforms of ARPC1 and ARPC5 across Jurkat cell line and primary human CD4 T cells from two representative healthy donors were verified using Western blotting. Representative immunoblots compare the protein levels of each subunit and their isoforms in CD4 T cells. Additional comparisons for expression of these proteins in Resting (R) and Activated (A) CD4 T cells from Donor 4 and 5 are shown, respectively. Black arrowheads indicate the specific bands, black asterisks mark unspecific bands. Note that the ARPC5L antibody also detects ARPC5 (marked by red asterisk).

Fig. 2. ARPC5 isoforms differentially regulate nuclear and plasma membrane actin polymerization. (**A**) Representative immunoblots show knockdown of ARPC1 and ARPC5 isoforms in JNLA.GFP cells treated with indicated shRNA. Black arrowheads indicate the specific bands, black asterisks mark unspecific bands. Note that the ARPC5L antibody also detects ARPC5 (marked by red asterisk). (**B**) Representative spinning disk confocal still images of JNLA.GFP cells treated with indicated shRNA, show post activation with P/I. Arrows point to the nuclear F-actin (NFA). (**C**) Quantification of NFA formation in shRNA treated cells relative to the scrambled control treated cells. Error bars were calculated from mean±SD of 4 independent experiments where 30 cells were analyzed per condition per experiment. Each dot represents mean of each independent experiment. (**D**) Representative single plane immunofluorescence images of Phalloidin-488 stained F-actin ring (AR) formation in JNLA.GFP cells treated with indicated shRNA upon activation on coverslips coated with antiCD3+CD28 antibodies. Arrowheads point to the f-actin ring at the PM. (**E**) Quantification of Phalloidin stained F-actin ring (AR) formation in shRNA treated cells relative to the control treated cells. Error bars were calculated from mean±SD of four independent experiments where at least 100 cells were analyzed per condition per experiment. Each dot represents mean of each independent experiment. One sample t-test was used to determine statistical significances, where $***P \leq 0.0002$ and *ns*: not significant. Scale bar, 5µm.

Fig. 3. Effects observed on nuclear and plasma membrane F-actin dynamics upon ARPC5/C5L knockout can be rescued by overexpression of the respective ARPC5 isoforms.

(**A**) Shown are representative confocal still images of the indicated KO JNLA.GFP cells overexpressing mCherry (control) or mCherry fusion proteins of an ARPC5 isoforms, post activation with either anti CD3+CD28 antibodies (top panel) or with P/I (bottom panel). Arrows point to the nuclear F-actin (NFA, bottom). Arrowheads point to the F-actin ring (top). Scale bar, 7µm. **(B)** Quantification of AR formation in the PM, stained with Phalloidin is compared to the NFA formation visualized with NLA-GFP in the indicated KO or KO+ARPC5 isoform expressing cells was performed relative to the non-targeting control (NTC) treated cells. 'mCherry' alone was used as vector backbone control for the overexpression study. Bars indicate mean from one independent

289 experiment where 30-50 cells were analyzed per condition. **(C)** Shown are representative spinning
290 disk confocal images of ARPC5.mCherry and ARPC5L.mCherry distribution in non-activated JNLA
291 cells. White arrows point to the respective C5 or C5L punctae in the nucleus. (**D**) Representative,
292 deconvoluted and segmented Stimulated emission depletion (STED) images show endogenous nuclear
293 actin filaments (stained with Phalloidin-647N) and ARPC5.mCherry/ARPC5L.mCherry (stained in
294 atto-594 channel) in A3.01 T cells, stimulated with P/I for 30s. MCherry fluorescence was enhanced
295 by staining with an anti-mCherry antibody followed by an Atto-568 coupled secondary antibody.
296 Arrows (in white) point to the colocalization events. Percent colocalization is mentioned as mean± SD
297 (in cyan) for each of the isoforms. Scale bar, 500nm.
298
299 **Fig. 4. Differential role of ARPC5 isoforms in replication stress mediated NFA formation (A)**
300 Schematic of KO generation and induction of replication stress in the JNLA KO cells using
301 Aphidicolin (APH). **(B)** Shown are representative spinning disk confocal still images of the APH pre-
302 treated KO or control cells. The movies were acquired for 5h with acquisition every 15min post pre-
303 treatment of cells with APH. The stills at the indicated timepoints are representative of the timepoint
304 where the NFA burst has been observed in each condition. **(C)** Quantification of the % of cells with
305 NFA bursts (first 2h of imaging) post replication stress induction in control and KO cells are shown
306 where the bars represent mean values from three independent experiments. Around 40-60
307 cells/condition/experiment where analyzed. Statistical significance was calculated using One-way
308 ANOVA (multiple comparison) **(D)** stacked bar graph (denoted by three different colors) shows the
309 maximum NFA burst within the first 2h of the entire 5h of live cell imaging duration. **(E)** JNLA cells
310 transduced with either mCherry (control) or CAMBP4.NLS-mCherry were pre-treated with solvent
311 control (DMSO), activated by PMA+Ionomycin (P/I) or replication stress induction by APH for 3h
312 prior to live cell imaging. Shown are representative spinning disk confocal still images (within the first
313 2h of imaging) of the DMSO control vs either P/I or APH mediated NFA bursts (white arrows) in the
314 presence and absence of nuclear Calmodulin. Movies for visualizing replication stress were acquired
315 for 5h with acquisition every 15min post pre-treatment of cells. Whereas movies for visualizing P/I
316 activation induced NFA were acquired for 5mins with acquisition every 15-30s. **(F)** Quantification of

317 the NFA bursts in the above-mentioned conditions were performed. Shown here are the bars
318 representing mean values from three independent experiments, where at least 30 cells were analyzed
319 per condition per experiment for NFA quantification. Statistical significance was calculated using
320 Welch's t-test. *$P \leq 0.0332$, **$P \leq 0.0021$, ***$P \leq 0.0002$ and ns: not significant. Scale bar, 7µm.
321 **(G)** Schematic model for the regulation of actin dynamics induced upon TCR engagement (left) or
322 induction of DNA replication stress by aphidicolin (APH) (right). See text for details.
323
324
325

STAR Methods

Cells and reagents

HEK 293T cells were cultured in DMEM high glucose plus 10% feline bovine serum (FBS, Milipore), 100U/mL penicillin and 100µg/mL streptomycin. Primary T cells, Jurkat Tag cells (JTAgs) and CLEM derived A3.01 cells were cultured in RPMI containing 10% FBS and 1% Penicillin-streptomycin and GlutaMAX-I (Gibco). All experiments performed in JTag cells stably expressing nuclear lifeact-GFP (JNLA) were obtained as described previously in [7]. All Cell lines were cultivated according to their ATCC (https://www.atcc.org) guidelines. For visualization of nuclear F-actin, A3.01 or JNLA were washed thoroughly with PBS, adjusted to a cell density of 3E5/ml, and incubated overnight in RPMI (phenol-Red free medium, GIBCO) containing 0.5% (A3.01) or 10% (JNLA) FBS. For Immunofluorescence (IF) microscopy: F-actin was stained with Phalloidin Alexa Fluor 488 or atto-AF488 (Thermo Fischer). Alexa antibodies for IF such as: goat anti-mouse Alexa Fluor 568, goat anti-rabbit Alexa Fluor 647 and goat anti-rabbit Alexa Fluor 568 were obtained from Thermo Fischer Scientific. The following anti-CD3 (clone HIT3a against CD3ε; BD Pharmingen) and mouse anti-CD28 (CD28.2, BD Pharmingen) were used at 1:100 dilution for coating coverslips/GBDs to make stimulatory surface for T cell activation. Other antibodies used were mouse-anti-ARP3, 1:10,000 (cloneFMS338, SIGMA), mouse-anti-GAPDH, 1:2500 (G9, Santa Cruz), mouse anti- p16-ARC, 1:500 (#305011, Synaptic systems & sc-166760, SCBT), rabbit anti-ARPC5L, 1:1000 (GTX120725 GeneTex and 22025-1-AP Proteintech), rabbit anti-ARPC1A, 1:500 (#HPA004334, Sigma), mouse anti-ARPC1B, 1:500 (SCBT), rabbit anti-ARPC2, 1:1000 (EPR8533 Abcam), mouse anti-ARPC3, 1:500 (#HPA006550, Sigma Aldrich), mouse anti-ARPC4, 1:500 (#NBP1-69003, Novus Biologicals), mouse anti-mCherry, 1:1000 for WB and 1:500 for IF (NBP1-96752), rabbit anti-mCherry, 1:1000 for

WB and 1:500 for IF (ab167453), rabbit anti-pTyr, 1:100 (#sc18182, SCBT), rabbit anti-pSLP76, 1:1000 (#ab75829, Abcam), HRP-coupled secondary rabbit or mouse antibodies for immunoblotting were obtained from Jackson Immuno Research was used at a dilution of 1:5000 for all samples. The secondary Alexa fluorescent coupled antibodies (either mouse or rabbit) used for IF staining were obtained from Invitrogen and used at a dilution of 1:1000.

For live cell imaging and STED microscopy: glass- bottom-dishes (GBD) with 35 mm plate diameter, 14 mm glass diameter, thickness 1.5 (Mattek corporation) and µ-slide 8-well glass bottom chambers (Ibidi) were used along with poly-lysine (Sigma), coated at a concentration of 0.01% in sterile filtered water. Phalloidin atto-647N used for STED imaging was bought from ATTO-TEC GmbH (AD 647N-81).

Preparation of primary CD4 T cells

For the isolation of primary human CD4 T cells, human Buffy Coats from anonymous healthy donors were obtained from the Heidelberg University Hospital Blood Bank. CD4+ T cells were isolated by negative selection with the RosetteSepTM Human CD4+ T Cell Enrichment Cocktail and separated by Ficoll gradient centrifugation, resulting in homogenous populations of CD4+ T cells with a purity of 90-95% as assured by flow cytometry. Cells labelled as 'Resting' were cultured for 72h in complete RPMI media containing recombinant human IL2 (Biomol #155400.10) at 10ng/ml final concentration. Whereas the cells labelled as 'Activated' were cultured for 72h in complete RPMI media containing recombinant human IL2 (Biomol #155400.10) at 10ng/ml final concentration along with dynabeads at a ratio of 25µl Dynabeads/10 million cells (#11132D, Gibco).

Agonists and inhibitors

The following chemicals were used at the indicated concentrations: Ionomycin (Iono, 2μM), Phorbol 12-myristate 13-acetate (PMA, 162 nM), CK-869 (100 μM), KN-93 (0.25 μM), KN-62 (2.5 μM), STO-609 (5μM) and Aphidicolin (15μM), all obtained from Sigma Aldrich.

Expression plasmids

pLVX vector expressing either human ARPC5/C5L cDNA fused to a mCherry fluorescent reporter or just the mCherry alone, were a kind gift from the lab of M.Way, generated as described in [14]. Plasmids expressing mCherry alone or mCherry conjugated to CAMBP4 in the pWPI backbone were used as described in Tsopoulidis et al and were selected using blasticidin (5μg/ml). For the stable expression of shRNAs, gene specific target sequences (available upon request) were cloned into the lentiviral Vector pLKO.1-puro (Addgene) as described in [7].

Live-cell imaging of actin dynamics

Live imaging of actin dynamics was performed with a Nikon Ti PerkinElmer UltraVIEW VoX spinning disc confocal microscope equipped with a perfect focus system (PFS), a 60X oil objective (numerical aperture, 1.49), Hamamatsu ORCA-flash 4.0 scientific complementary metal-oxide semiconductor camera, and an environmental control chamber (37°C, 5% CO2), as described earlier in [7]. Acquisition settings varied depending on the total acquisition time required for each experimental question/setup. The following are the acquisition settings for short term imaging: exposure time, 300 ms; frame rate, 6 to 10 frames/s, number of Z planes, 10; Z-stack spacing, 0.5μm; 488 nm, laser power between 4.5-5.5%; and total acquisition time, 3 to 10 min. Jurkat cells stably expressing nuclear lifeact.GFP (JNLA) were always washed with PBS and split 24 hours before the experiment to a density of 3×10^5/ml. The next day, 3×10^5 cells were harvested, washed with PBS, and resuspended in 100μl reconstituted RPMI containing 10% FCS. For imaging the actin

dynamics of JNLA cells falling on stimulatory surface (coated with anti-CD3+CD28 antibodies), the PFS system was adjusted first with a low amount of highly diluted cells placed on the coated glass bottom dish. A single cell was centered to the field of view, and the PFS was adjusted to automatically focus on the glass-cell contact site. Subsequently, the stage was moved to a cell-free area, and 100µl of the cell suspension (3×10^5/100µl) was added to the glass bottom dish with simultaneously recording cells while making contact with the glass surface.

For imaging of actin dynamics in cells resting on the glass surface, 100µl of cells (3×10^5/ml) was plated on polyK-coated glass-bottom dishes, allowed to adhere for 5 min, and then stimulated with PMA/Iono in RPMI media.

Super resolution imaging of nuclear actin

A3.01 T lymphoblastoid cells were washed and adjusted to cell density of 0.35 million cells/ml a day prior to the experiment, as described above. The next day, 0.6 million cells were collected/well of a 8-well chambered dish, washed once with PBS and resuspended in of RPMI (phenolRED free) containing 0.5% FBS. Cells were allowed to adhere for 5 min on polyK-coated 8-well chamber glass bottom dish. Stimulation was performed by adding 100 µl of PMA/Iono solution dropwise to the cell suspension. Cells were activated for 30s and then permeabilized and stained with 100µl Perm solution containing 0.3% Triton X-100 + Phalloidin -Alexa Fluor 488 (1:2000) in 1X cytoskeleton buffer [10 mM MES, 138 mM KCl, 3 mM MgCl, 2 mM EGTA, and 0.32 M sucrose (pH 6.1)] for 30s. Cells were fixed with 1 ml of 4% methanol-free formaldehyde (Pierce) in 1X cytoskeleton buffer and incubated for 25 min at RT in the dark. Subsequently, the fixed cells were washed twice with cytoskeleton buffer, blocked with 5% bovine serum albumin (BSA) prepared in 1X cytoskeleton buffer, and stained with 1:500 Phalloidin atto-647N in 1X cytoskeleton buffer for 1 hour at room temperature (RT) or overnight (ON) at 4°C. Additionally, to enhance the mCherry signal of

the C5/C5L-mCherry expression constructs in the cells, primary antibody staining using anti-mCherry antibody (1:500) was performed ON in blocking buffer as mentioned above. This was followed by multiple washing steps in 1X cytoskeleton buffer and staining with secondary antibody conjugated with an Atto-568 dye, for 1h at RT. Phalloidin atto-647N was added at this step with the secondary antibody to stain the endogenous nuclear actin filaments, which were observed in ~40-60% of the cells.

STED microscopy was performed on an Expert Line STED system (Abberior Instruments GmbH, Göttingen, Germany) equipped with an SLM-based easy3D module and an Olympus IX83 microscope body, using a 100x oil immersion objective (NA, 1.4; Olympus UPlanSApo). STED images were acquired using the 590 nm (ARPC5/ARPC5L signals) and 640 nm (actin filament signals) excitation laser lines in the line sequential mode with corresponding 615/20 and 685/70 emission filters placed in front of avalanche photodiodes for detection. 775 nm STED laser (15% of the maximal power of 3 mW) was used for depletion with pixel dwell time of 10 to 15 µs, 15 nm xy sampling and 9x accumulation. To increase the signal-to-noise and facilitate subsequent image segmentation and quantification, STED images were restored with Huygens Deconvolution (Scientific Volume Imaging) using Classic Maximum Likelihood Estimation (CMLE) algorithm and Deconvolution Express mode with “Conservative” settings.

To segment actin filaments and ARPC5/ARPC5L signals in obtained STED images we trained a Random Forest classifier using ilastik (ref PMID: 31570887) autocontext workflow which predicts semantic class attribution (signal or background) for every pixel. The training set of data was arbitrary selected and very sparsely labelled (<0.1% of total pixels were manually categorized into “signal” and “background” categories). Obtained machine learning algorithm was used applied to all acquired images ensuring an unbiased signal segmentation across all experiments. This allowed the quantification of the number of ARPC5/ARPC5L

452 signals colocalizing with nuclear actin filaments by visual inspection of binary (segmented)
453 images.
454
455 **Imaging actin dynamics at the Immune synapse post CK-inhibitor treatment**
456 Raji B cells were stained with Cell trace Deep Red (10µM, Thermo Fischer) at 1:1000
457 dilution for 1h and simultaneously loaded with Staphylococcal enterotoxin E (SEE, Toxin
458 Technology) at a concentration of 5 µg/ml, in RPMI complete media for 30 min at 37°C and
459 subsequently washed and resuspended in 10% FBS containing RPMI at a concentration of
460 $5x10^4$ cells in 100µl. JNLA cells were washed and adjusted a day before as described above.
461 24h later $1x10^6$ were harvested, washed in PBS and resuspended in 100µl RPMI complete
462 media containing either DMSO or the CK869 for 1h at 37°C. The media is replenished after
463 1h with fresh media containing either the solvent or the inhibitor such that the cells are at a
464 final density of $5x10^4$ cells in 100µl. 100µl of the treated JNLA cells are plated on a poly-
465 lysine coated GBDs. Approx. 5-10 regions on the GBDs were selected for live cell imaging
466 using the spinning disk confocal microscopy as described above. Imaging was started and
467 100µl Raji B cells were added dropwise onto the T cell suspension while the image
468 acquisition was ongoing. The following are the acquisition settings for the imaging: exposure
469 time, 300 ms; frame rate, 6 to 10 frames/s, number of Z planes, 3; Z-stack spacing: 1-1.5µm;
470 488 nm, laser power 5.5%; and total acquisition time, 30min with acquisition every 30s/XY
471 position.
472
473 **RNA extraction and Quantitative PCR (qPCR)**
474 For RNA extraction NucleoSpin RNA II kit (Macherey-Nagel) was used. $10x10^6$ cells were
475 collected per condition/per cell line, washed with cold PBS once and their pellets were stored
476 at -80°C for maximum 2-3weeks. RNA extraction was done following manufacturer's
477 protocol. After RNA quantification by UV/VIS spectrometry (Nanodrop), between 500ng-

1000ng of total RNA was reverse transcribed using the SuperScriptII (Invitrogen) according to the manufacturers' instructions. 1:10 dilution of the cDNA in RNAse free water was used for qPCR reaction using the SYBR green PCR master mix (Life Technologies), and reactions were performed on a Quant Studio1 sequence detection system (Applied Biosystems) using the following program: 50°C for 2 min, 95°C for 10 min, and 40 cycles of 95°C for 15 s and 60°C for 1 min. GAPDH (glyceraldehyde-3-phosphate dehydrogenase) mRNA was used for normalization of input RNA wherever needed or mentioned. The primers used are available upon request.

Immunoblot analysis

1xE6 cells/condition were collected and lysed in lysis buffer (50 mM Tris-HCl [pH 7.4], 75 mM NaCl, 1 mM EDTA, 1 mM NaF, and 0.5% NP-40) with a freshly added protease inhibitor cocktail and sodium vanadate and subjected to 9 cycles (30s ON-10s OFF) of ultrasonication (Bioruptor Plus; Diagenode). The sonicated samples are then spun down, and the supernatant is collected for protein estimation using the microBCA kit (Pierce). 15-30µg of protein is then mixed with 6X sample buffer (10% sucrose, 0.1% bromophenol blue, 5 mM EDTA [pH 8.0], 200 mM Tris [pH 8.8]), and boiled at 95°C for 10min. The lysates are then run on 12% SDS-PAGE gel and blotted with Trans-blot PVDF membranes (BioRad) for 10min, blocked in 5% BSA in TBS-T and probed with the following primary antibodies: mouse anti-ARP3, mouse anti-GAPDH, rabbit anti-GAPDH, mouse anti-ARPC5, rabbit anti-ARPC5L, mouse anti-ARPC1B, rabbit anti-ARPC1A, rabbit anti-ARPC2, mouse anti-ARPC3, mouse anti-ARPC4 as mentioned in the reagent section. Secondary antibodies conjugated to HRP were used for enhanced chemiluminescence (ECL)-based detection.

Lentivirus production

For small scale production of lentiviral vectors containing shRNA constructs or the pLVX-expression plasmids, $3x10^5$ HEK 293T cells were seeded per 6-cm dish (2 ml media per well) 24 h before transfection. Transfection was performed using JetPEI (VWR International) with 1.5 µg of Vector DNA, 1 µg of psPAX2, and 0.5 µg of vesicular stomatitis virus G protein plasmid (pMD2.G) and 0.2 µg pAdvantage per well of a 6-well. Virus supernatants were harvested after 48 h, filtered through 0.45-µm-pore-size filters (Roth), and used immediately for transduction.

For the generation of stable T cell lines expressing the C5/C5L-mCherry constructs or primary human T cells expressing the Lifeact-GFP constructs, five 15 cm petri dishes were prepared with 2.5 x 106 HEK293T cells/dish in 22.5 ml medium. The transduction solution was prepared in a 50 ml reaction tube, containing: 112.5 µg vector, 40 µg (pMD2.G), 73 µg psPAX2, 25 ml NaCl and 500 µl JetPEI. The transduction solution was mixed and incubated at RT for 20min. For every dish 5ml of the solution was used. The dishes were incubated for 4 h at 37°C before changing the media. The supernatant containing virus particles was collected after 48h and filtered via 0.45 µm filter (Roth/Millipore). Virus was concentrated using 20% sucrose and ultracentrifugation at 24,000 rpm (Beckman SW28 rotor) for 2h at 4 °C. The supernatant was discarded and 200 µl fresh FCS free RPMI medium were added on the virus pellet and incubated for 30 min at 4 °C. The pellet was resuspended and stored at –80°C or directly used for transduction. Virus titers were assessed by determination of reverse transcriptase activity (SG-PERT).

Transduction of human T cells

$2\text{-}3x10^6$ JNLA or A3.01 cells were resuspended in 1.5E11 puRT/ µl concentrated virus solution or 1 ml of non-concentrated virus supernatant followed spin-transduction in 24-well plate format at 2300 rpm, for 1.5 h at 37°C, RT. After transduction the cells were incubated at

37 °C, overnight. The next day the cells were transferred into a 12-well plate and 3 ml complemented RPMI medium was added and incubated overnight. Cells expressing shRNAs or the C5/C5L-mCherry constructs were transferred to fresh medium 24h post transduction. 48h later puromycin (1.5µg/ml) was added and 72h post transduction, the medium was changed to fresh media with puromycin to accelerate cell growth. On day 4 post transduction, the cells were adjusted to the densities required according to the experimental question being addressed, with RPMI media without any selection antibiotics. Knock down was stable in the bulk culture for up to ~1week post transduction. To generate stable A301 cells expressing either C5 or C5L tagged with N-terminal mCherry, the cells were FACS sorted for mCherry expressing cells post selection with puromycin for 1 week and then expanded in culture.

Immunofluorescence Microscopy

As described previously [7], to study the actin dynamics in JNLA cells activated on stimulatory coverslips, 1-2x 10^5 cells are put on the stimulatory coverslips for 5min at 37°C before fixing them with 3% PFA. Following permeabilization and blocking, coverslips are incubated with primary antibodies overnight at 4°C in 1% BSA(PBS). For phospho-specific targets/antibodies, all steps were done in 1X TBS. Following dilutions are used for the primary antibodies: rabbit anti-pTyr (1:100), rabbit anti-pSLP76 (1:1000) and mouse anti-mCherry (1:500). Species specific secondary antibodies conjugated to Alexa-Flour 568/647 (1:1000) were used for along with Phalloidin-Alexa Fluor 488 (1:600) for staining the F-actin. Coverslips were mounted with Mowiol (Merck Millipore) and analyzed by either epifluorescence microscopy (IX81 SIF-3 microscope and Xcellence Pro software; Olympus) or confocal microscopy (TCS SP8 microscope and LAS X software; Leica).

Generation of CRISPR-Cas9 based Knockout cells

We designed two-three guideRNAs for knocking out each of the genes, ARPC5 and ARPC5L, respectively, with the help of Synthego's CRISPR design tool (https://design.synthego.com/#/). The guideRNAs were premixed with Cas9.3NLS (IDT) to create ribonucleoprotein complexes (RNPs) for faster and better editing efficiency as described earlier [27]. Premixed RNPs were then nucleofected (Nucleofector 4D, Lonza) into either the JNLA cells or primary CD4 T cells (human). JNLA cells post nucleofection are maintained in RPMI containing 10% FBS as a heterogenous pool, followed by knockout (KO) validation in the bulk pool using immunoblotting or flow cytometry.

Nuclear and cytoplasmic biochemical fractionation

JNLA cells were fractionated using the REAP method as described in [28]. $8x10^6$ cells were harvested for each condition. The only difference we adapted is the manual sonication instead of an automated one. The number of sonication cycle varies between 10-15 (60s ON, 10s OFF) with the manual sonicator at 4°C or with ice. Each of the nuclear, cytoplasmic and total cell fractions are then immunoblotted as described above. As and when necessary, immunoblots were often stripped in 1X stripping buffer, followed by blocking for 1h at RT and re-probing with primary antibodies ON at 4℃. The protocol we followed for stripping including the preparation of stripping buffer were adapted from Abcam's published protocol online (https://www.abcam.com/ps/pdf/protocols/stripping%20for%20reprobing.pdf).

Supplemental information

Supplementary Videos

Suppl. Video 1: Live NFA and AR formation in DMSO treated Jurkat CD4 T cells upon falling on a stimulatory surface.

Suppl. Video 2: Live NFA and AR formation in CK869 treated Jurkat CD4 T cells upon falling on a stimulatory surface.

Suppl. Video 3: Live imaging of an IS formation between DMSO treated JNLA (in grey) and SEE treated B cells (in magenta).

Suppl. Video 4: Live imaging of an IS formation between CK869 treated JNLA (in grey) and SEE treated B cells (in magenta).

Supplementary Figures

Suppl. Fig 1: Gene expression profile of Arp2/3complex subunits in CD4 T cells

(A) mRNA expression of all the subunits of the Arp2/3 complex along with the isoforms of ARPC1 and ARPC5 across Jurkat cell line and primary human CD4 T cells were additionally verified. The heatmap shows the mRNA expression levels of each of the human ARP2/3 complex subunits and their isoforms, as analyzed by the Ct mean values using qRT-PCR. Color code for the heatmap: dark (high expression) and white (low expression). D1-D5 indicates CD4 T cells isolated from five different healthy human donors. Comparison of gene expression between RNA isolated from naïve CD4 T cells (denoted as Resting) and from the CD4s that post activated for 72h with Dynabeads (denoted here as Activated 'A').

Suppl. Fig 2: ARPC5 knockdown cells exhibit filopodia and lamellipodia like extensions upon TCR activation.

(A) Representative bigger field of view of single plane immunofluorescence images showing Phalloidin-488 stained F-actin ring (AR) formation in JNLA.GFP cells, treated with indicated shRNA upon activation on coverslips coated with antiCD3+CD28 antibodies. Scale bar, 10µm.

(B) Representative confocal still images (maximum projection) of JNLA.GFP cells upon activation for 5min on stimulatory coverslip leads to formation of distinct morphologies of actin ring formation and cell spreading. Cells were fixed, permeabilized and stained for F-actin (with Phalloidin 488) and counterstained with Dapi. **(C-D)** Cells with knockdown, exhibiting different morphologies (bars in different colors, stacked) as classified above in (B), upon TCR activation, were quantified as % of cells of the total 100 cells/condition is represented in (C). **(D)** shows the fold change in the different morphotypes exhibited by the cells upon knockdown relative to the control cells. Scale bar, 10µm.

(E) Representative still images from live cell spinning disk acquisition of JNLA.GFP cells with control and C5/C5L knockdown, upon falling on stimulatory GBDs, form NFA and AR. Movies were acquired for at a frame interval of 30s for a total of 10min after the T cells were added dropwise. Two timepoints representing early activation-NFA formation and a later timepoint showing AR formation for each condition has been shown. Arrows (in white) points at the NFA whereas arrowheads (in white) point at the AR formation as it starts forming (top panel) or has fully formed into a classical actin ring structure (bottom). Scale bar, 7µm **(F)** Fold change was calculated for frequency of NFA (black bars) and AR formation (grey bars) for C5/C5L knockdown relative to control samples upon TCR activation on stimulatory surface. At least 30cells/condition/experiment were analyzed. Bar graph shows the mean of two independent experiments with dots representing each experiment.

Suppl. Fig 3: Rescue of the NFA and AR upon overexpression of the ARPC5 isoforms in JNLA Knockout cells.

(A) Representative immunoblots show levels of each of the ARP2/3 complex subunits in JNLA.GFP cells with the indicated knockout (KO) of each of the ARPC5 isoforms. Black arrowheads indicate the specific bands, black asterisks mark unspecific bands. Note that the ARPC5L antibody also detects ARPC5 (marked by red asterisk). Immunoblots are representative of three independent experiments. **(B-C)** Shown are representative immunoblots confirming the successful overexpression of each of the ARPC5 isoforms in JNLA.GFP cells with the indicated knockout (KO) of each of the ARPC5 isoforms compared to the nontargeting control (NTC) cells.

Suppl. Fig 4: ARPC5 KO impacts the proximal TCR activation via Tyr and SLP-76.

(A,D) Representative confocal images of JNLA.GFP cells with indicated knockout or control (NTC), upon 5min of activation on coverslips coated with anti-CD3+CD28 antibodies. Cells were fixed and stained for F-actin (with Phalloidin 488) and pTyr or pSLP-76 (AlexaFluor 647), respectively. **(B,E)** shows quantification of the total number of pTyr or pSLP-76 clusters/cell in KO relative to control cells analysed using the 'Spot Detector' Fiji plugin. **(C,F)** Dot plots represent the changes in overall intensity of pTyr or pSLP-76 clusters per cell where each dot represents intensity of clusters/cell analysed. Error bars were calculated from meanSD of 3 independent experiments where ~80-100 cells were analyzed per condition. One sample t-test was used to determine statistical significances, where *P $\leq$ 0.033, **P $\leq$ 0.0021, ***P $\leq$ 0.0002 and ns: not significant. Scale bar, 7µm. **(D)** Subcellular distribution of the ARPC5 subunit and its isoform ARPC5L was determined by performing a biochemical fractionation of JNLA CD4 T cells. Representative immunoblots reveal levels of ARPC5 isoforms along with ARP3 in the whole cell extract (WCE), cytoplasmic (C) and nuclear (N) fractions in the indicated JNLA.GFP knockout cells post fractionation. Arp3 was used as an additional reference for the Arp2/3 complex. **(E)** The dot plot shows frequency of colocalization of ARPC5 and ARPC5L with nuclear F-actin (from representative STED- super resolved images shown in Fig3D) in A3.01 cells post 30s of stimulation with PMA+Ionomycin. Each dot represents colocalization events per cell that was analysed.

Suppl. Fig 5: APH mediated vs P/I mediated NFA burst in CD4 T cells.

(A) Representative immunoblots shows induction of phospho levels of DNA damage sensor CHK-1 in JNLA.GFP cells upon replication stress induction by Aphidicolin (15µM, APH) for 3h. Membranes were first probed with phospho specific antibodies, followed by stripping and re-probing with antibodies against total protein and GAPDH. Immunoblots are representative of three independent experiments. **(B)** Single cell tracking of 10 cells per condition (denoted by different colors for NTC, C5 or C5L KO) for the entire timeframe of 5h post pre-treatment with APH, shows the APH mediated NFA kinetics in KO and control JNLA cells. **(C)** shows relative comparison (Fold change, FC) of cells forming either NFA or AR, respectively, in Control and KO JNLA cells upon two different modes of

T cell activation i.e., activation with PMA+Ionomycin (P/I) or on anti CD3/28 coated coverslips. Bars represent mean values from three independent experiments and error bars were calculated from mean±SD of 3 independent experiments where at least 30 cells were analyzed per condition per experiment for NFA quantification and more than 100 cells per condition per experiment were analyzed for AR quantification. **(D)** Blocking of the calcium signalling pathway downstream of Calmodulin, using inhibitors STO609, KN93 and KN62, respectively on JNLA cells, followed by induction of replication stress with APH does not impair the replication stress mediated NFA bursts. 30 cells/ condition were analyzed. Statistical significance was calculated using One-way ANOVA (multiple comparison) or Welch's t-test according to the experimental setup. *$P \leq 0.0332$, **$P \leq 0.0021$, ***$P \leq 0.0002$, ****$P \leq 0.000021$ and ns: not significant.

References

1. Schrank, B.R., Aparicio, T., Li, Y., Chang, W., Chait, B.T., Gundersen, G.G., Gottesman, M.E., and Gautier, J. (2018). Nuclear ARP2/3 drives DNA break clustering for homology-directed repair. Nature *559*, 61-66.

2. Caridi, C.P., D'Agostino, C., Ryu, T., Zapotoczny, G., Delabaere, L., Li, X., Khodaverdian, V.Y., Amaral, N., Lin, E., Rau, A.R., et al. (2018). Nuclear F-actin and myosins drive relocalization of heterochromatic breaks. Nature *559*, 54-60.

3. Caridi, C.P., Plessner, M., Grosse, R., and Chiolo, I. (2019). Nuclear actin filaments in DNA repair dynamics. Nat Cell Biol *21*, 1068-1077.

4. Lamm, N., Read, M.N., Nobis, M., Van Ly, D., Page, S.G., Masamsetti, V.P., Timpson, P., Biro, M., and Cesare, A.J. (2020). Nuclear F-actin counteracts nuclear deformation and promotes fork repair during replication stress. Nat Cell Biol *22*, 1460-1470.

5. Pinzaru, A.M., Kareh, M., Lamm, N., Lazzerini-Denchi, E., Cesare, A.J., and Sfeir, A. (2020). Replication stress conferred by POT1 dysfunction promotes telomere relocalization to the nuclear pore. Genes Dev *34*, 1619-1636.

6. Baarlink, C., Wang, H., and Grosse, R. (2013). Nuclear actin network assembly by formins regulates the SRF coactivator MAL. Science *340*, 864-867.

7. Tsopoulidis, N., Kaw, S., Laketa, V., Kutscheidt, S., Baarlink, C., Stolp, B., Grosse, R., and Fackler, O.T. (2019). T cell receptor-triggered nuclear actin network formation drives CD4(+) T cell effector functions. Sci Immunol *4*.

8. Valitutti, S., Dessing, M., Aktories, K., Gallati, H., and Lanzavecchia, A. (1995). Sustained signaling leading to T cell activation results from prolonged T cell receptor occupancy. Role of T cell actin cytoskeleton. J Exp Med *181*, 577-584.

9. Sedwick, C.E., Morgan, M.M., Jusino, L., Cannon, J.L., Miller, J., and Burkhardt, J.K. (1999). TCR, LFA-1, and CD28 play unique and complementary roles in signaling T cell cytoskeletal reorganization. J Immunol *162*, 1367-1375.

10. Acuto, O., and Cantrell, D. (2000). T cell activation and the cytoskeleton. Annu Rev Immunol *18*, 165-184.

11. Reicher, B., and Barda-Saad, M. (2010). Multiple pathways leading from the T-cell antigen receptor to the actin cytoskeleton network. FEBS Lett *584*, 4858-4864.

12. Millard, T.H., Behrendt, B., Launay, S., Futterer, K., and Machesky, L.M. (2003). Identification and characterisation of a novel human isoform of Arp2/3 complex subunit p16-ARC/ARPC5. Cell Motil Cytoskeleton *54*, 81-90.

13. Galloni, C., Carra, D., Abella, J.V.G., Kjær, S., Singaravelu, P., Barry, D.J., Kogata, N., Guérin, C., Blanchoin, L., and Way, M. (2021). MICAL2 enhances branched actin network disassembly by oxidizing Arp3B-containing Arp2/3 complexes. J Cell Biol *220*.

14. Abella, J.V., Galloni, C., Pernier, J., Barry, D.J., Kjær, S., Carlier, M.F., and Way, M. (2016). Isoform diversity in the Arp2/3 complex determines actin filament dynamics. Nat Cell Biol *18*, 76-86.

15. von Loeffelholz, O., Purkiss, A., Cao, L., Kjaer, S., Kogata, N., Romet-Lemonne, G., Way, M., and Moores, C.A. (2020). Cryo-EM of human Arp2/3 complexes provides structural insights into actin nucleation modulation by ARPC5 isoforms. Biol Open *9*.

16. Fäßler, F., Dimchev, G., Hodirnau, V.V., Wan, W., and Schur, F.K.M. (2020). Cryo-electron tomography structure of Arp2/3 complex in cells reveals new insights into the branch junction. Nat Commun *11*, 6437.

17. Pizarro-Cerda, J., Chorev, D.S., Geiger, B., and Cossart, P. (2017). The Diverse Family of Arp2/3 Complexes. Trends Cell Biol *27*, 93-100.

18. Monks, C.R., Freiberg, B.A., Kupfer, H., Sciaky, N., and Kupfer, A. (1998). Three-dimensional segregation of supramolecular activation clusters in T cells. Nature *395*, 82-86.

19. Grakoui, A., Bromley, S.K., Sumen, C., Davis, M.M., Shaw, A.S., Allen, P.M., and Dustin, M.L. (1999). The immunological synapse: a molecular machine controlling T cell activation. Science *285*, 221-227.

20. Campi, G., Varma, R., and Dustin, M.L. (2005). Actin and agonist MHC-peptide complex-dependent T cell receptor microclusters as scaffolds for signaling. J Exp Med *202*, 1031-1036.

21. Dustin, M.L., Tseng, S.Y., Varma, R., and Campi, G. (2006). T cell-dendritic cell immunological synapses. Curr Opin Immunol *18*, 512-516.

22. Varma, R., Campi, G., Yokosuka, T., Saito, T., and Dustin, M.L. (2006). T cell receptor-proximal signals are sustained in peripheral microclusters and terminated in the central supramolecular activation cluster. Immunity *25*, 117-127.

23. Monaco, S., Jahraus, B., Samstag, Y., and Bading, H. (2016). Nuclear calcium is required for human T cell activation. J Cell Biol *215*, 231-243.

24. Le Clainche, C., Schlaepfer, D., Ferrari, A., Klingauf, M., Grohmanova, K., Veligodskiy, A., Didry, D., Le, D., Egile, C., Carlier, M.F., et al. (2007). IQGAP1 stimulates actin assembly through the N-WASP-Arp2/3 pathway. J Biol Chem *282*, 426-435.

25. Suzuki, T., Mimuro, H., Suetsugu, S., Miki, H., Takenawa, T., and Sasakawa, C. (2002). Neural Wiskott-Aldrich syndrome protein (N-WASP) is the specific ligand for Shigella VirG among the WASP family and determines the host cell type allowing actin-based spreading. Cell Microbiol *4*, 223-233.

26. Miki, H., Miura, K., and Takenawa, T. (1996). N-WASP, a novel actin-depolymerizing protein, regulates the cortical cytoskeletal rearrangement in a PIP2-dependent manner downstream of tyrosine kinases. Embo j *15*, 5326-5335.

27. Albanese, M., Ruhle, A., Mittermaier, J., Mejías-Pérez, E., Gapp, M., Linder, A., Schmacke, N.A., Hofmann, K., Hennrich, A.A., Levy, D.N., et al. (2022). Rapid, efficient and activation-neutral gene editing of polyclonal primary human resting CD4(+) T cells allows complex functional analyses. Nat Methods *19*, 81-89.

28. Suzuki, K., Bose, P., Leong-Quong, R.Y., Fujita, D.J., and Riabowol, K. (2010). REAP: A two minute cell fractionation method. BMC Res Notes *3*, 294.

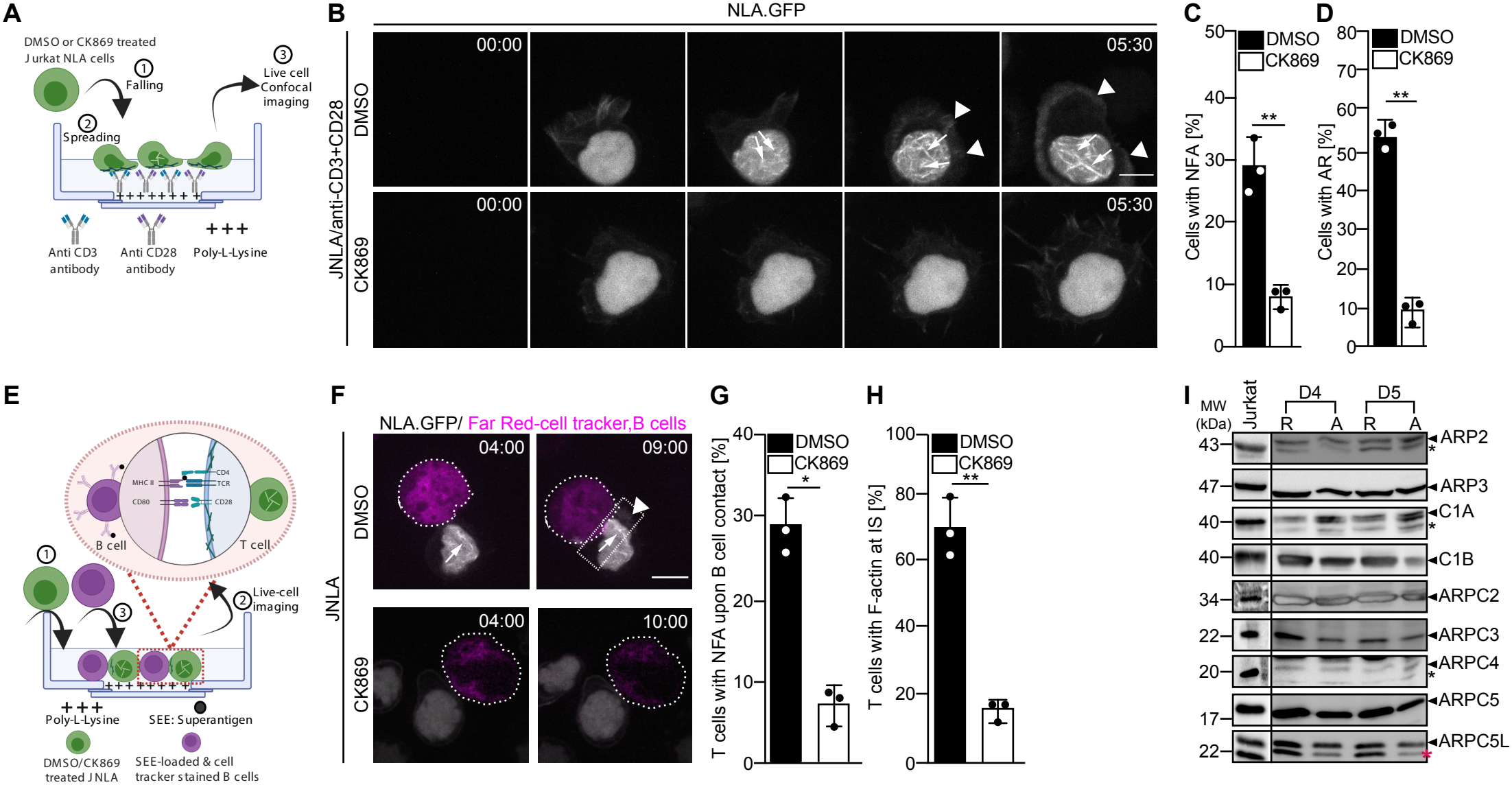

Sadhu et al., 2021: Fig.1

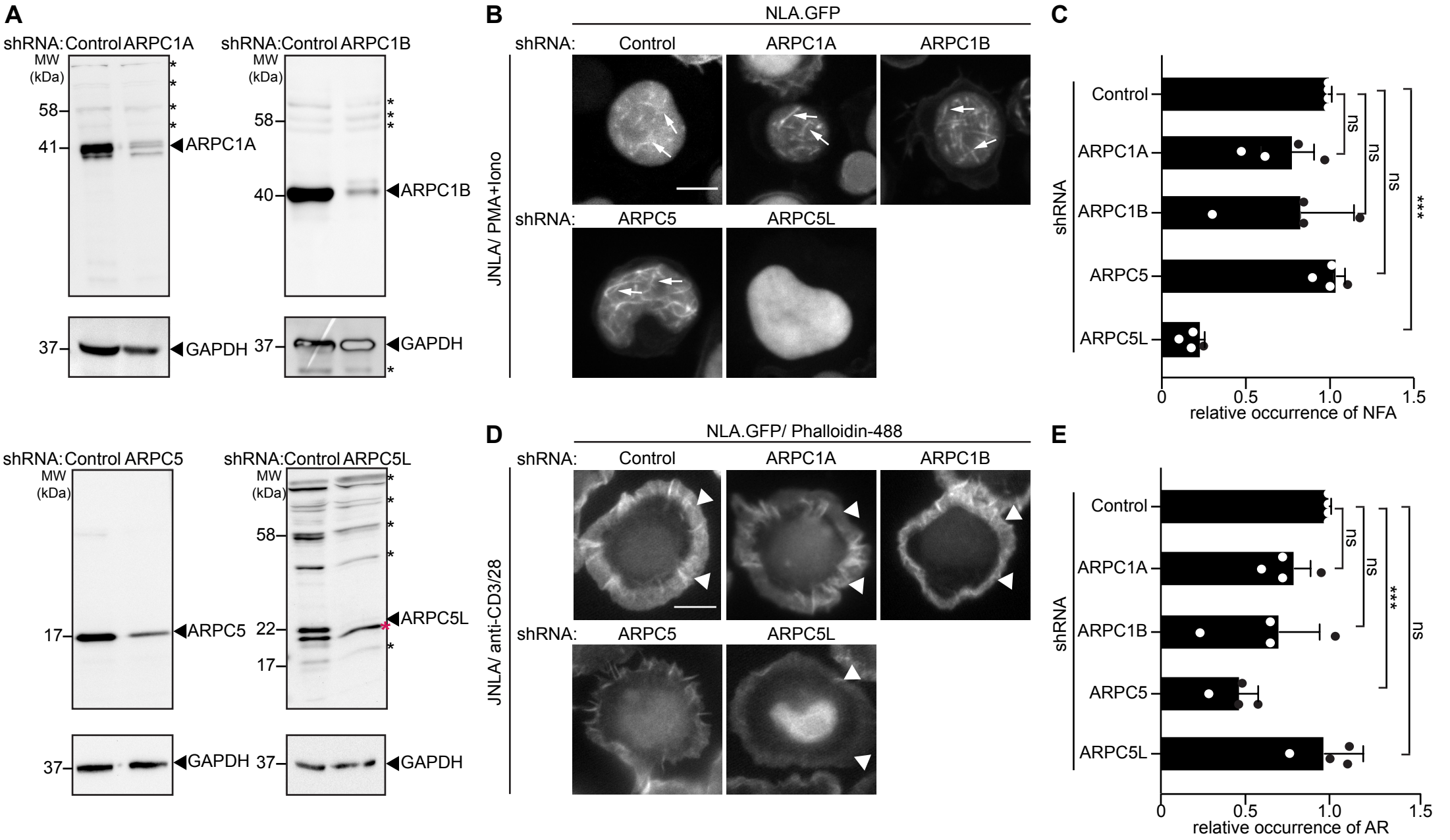

Sadhu et al., 2021: Fig.2

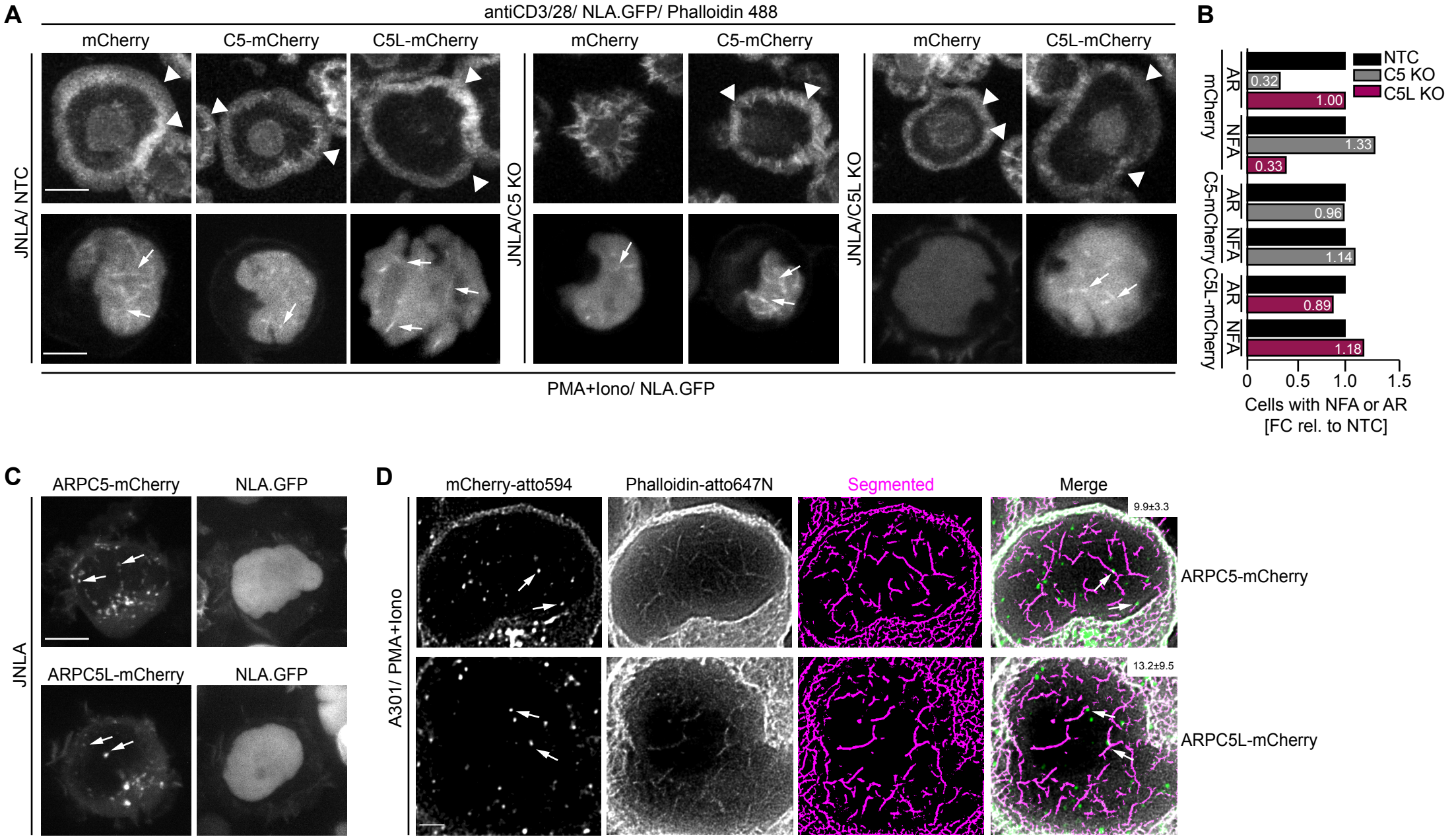

Sadhu et al., 2021: Fig.3

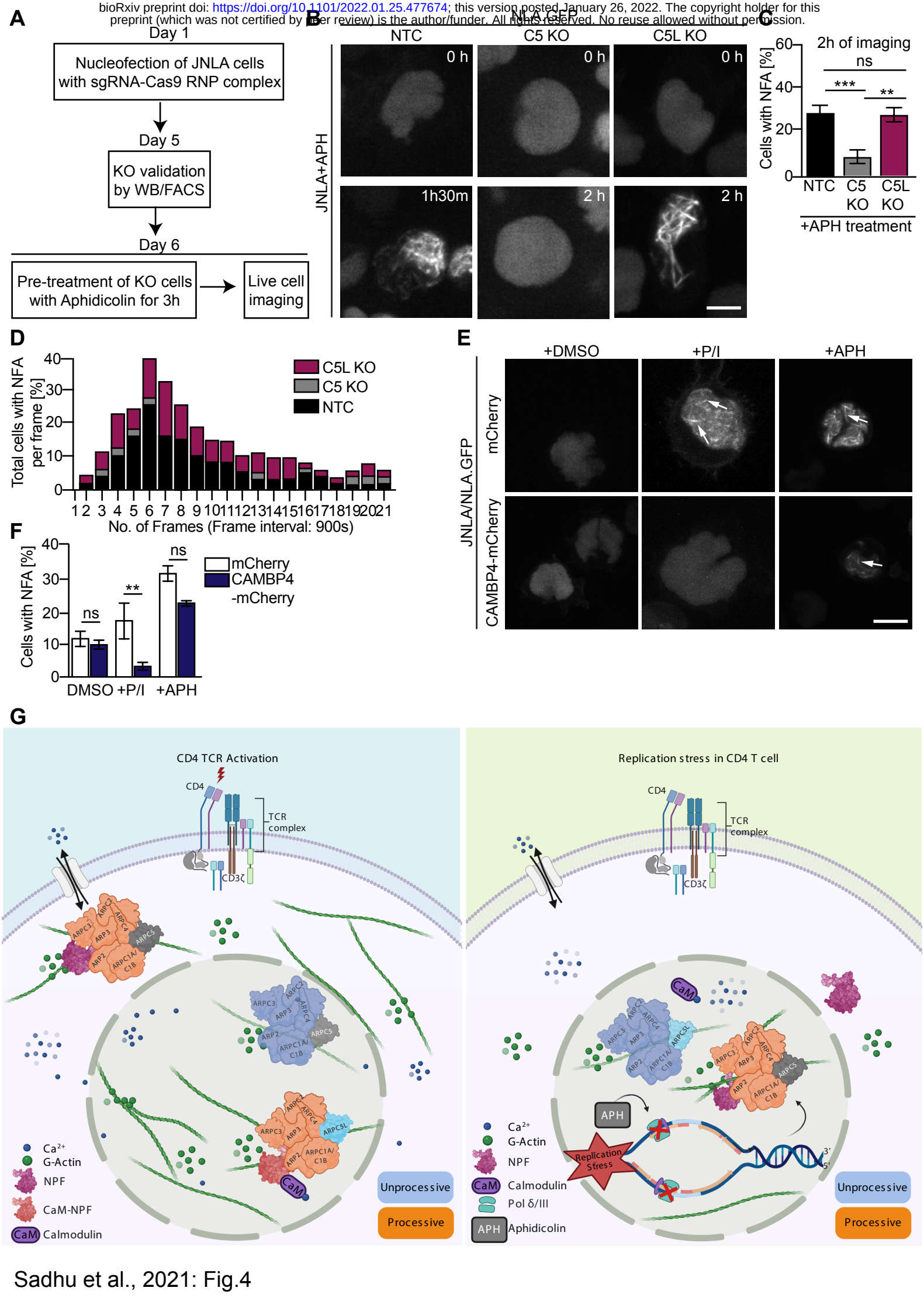

Sadhu et al., 2021: Fig.4

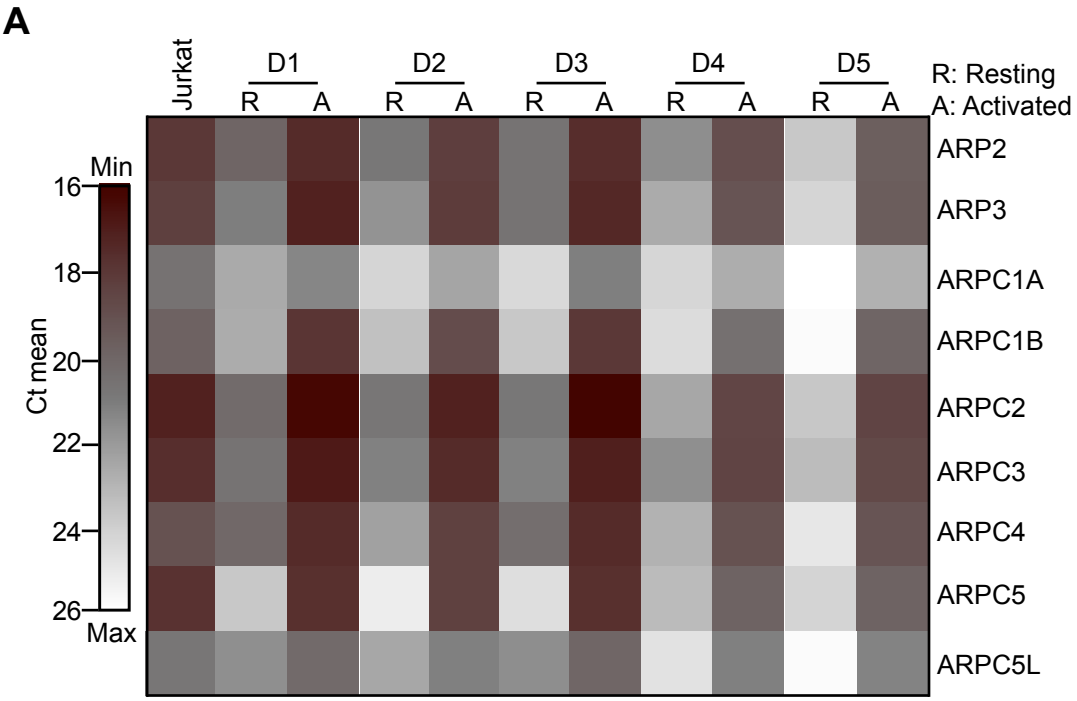

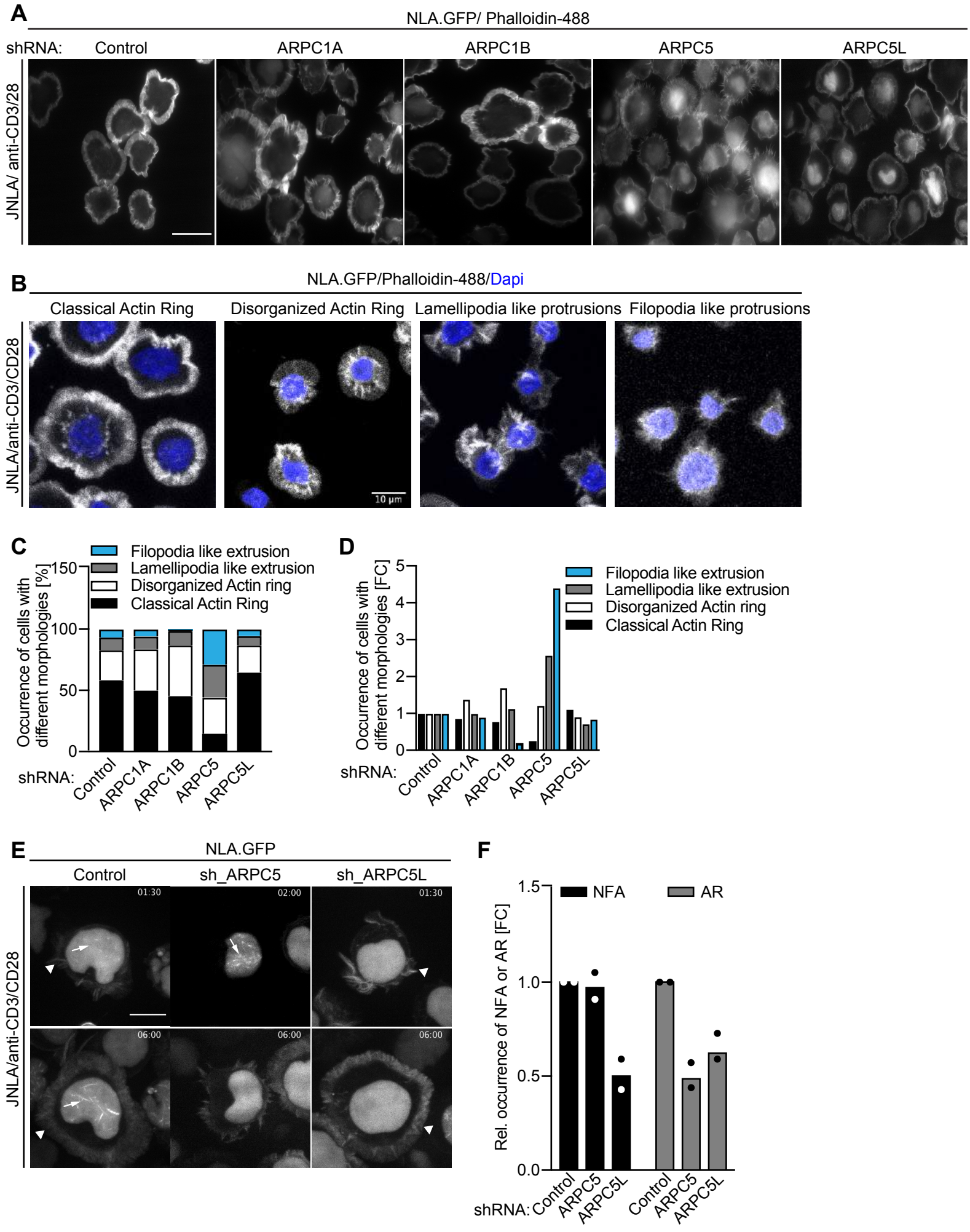

Sadhu et al., 2021: Suppl.Fig.2

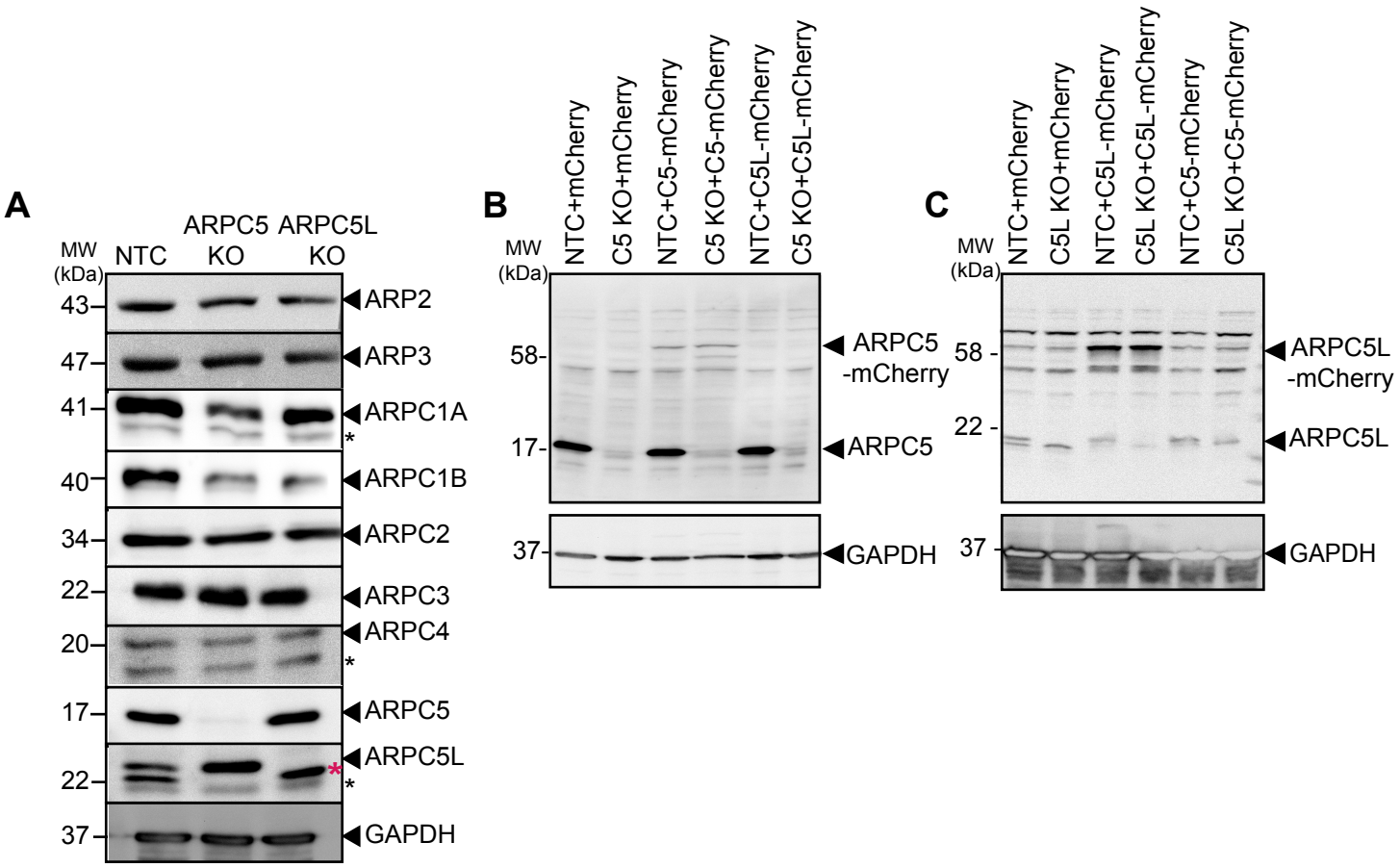

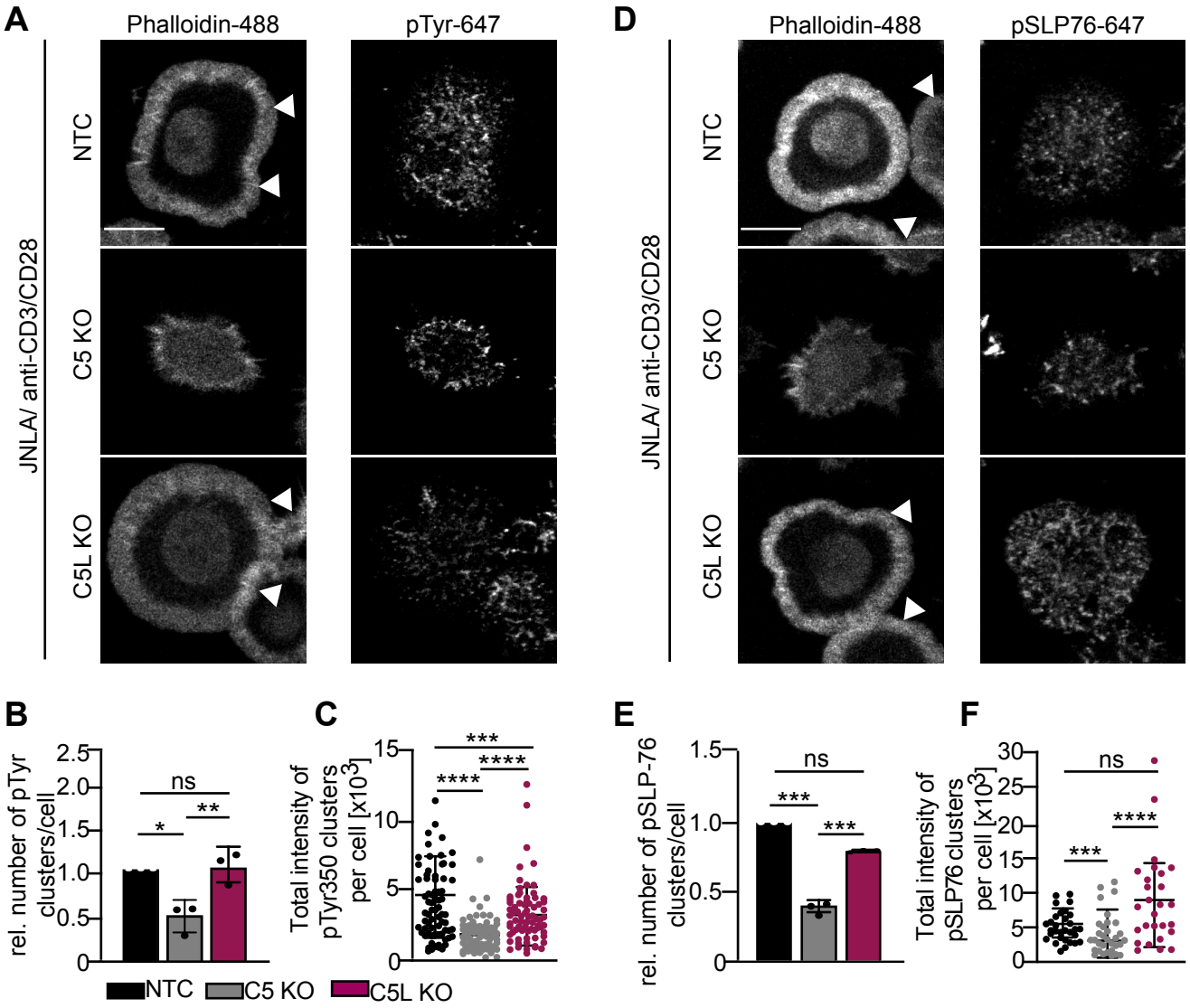

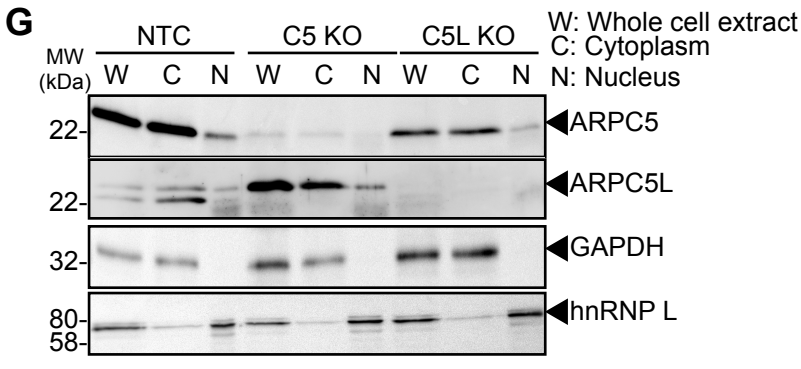

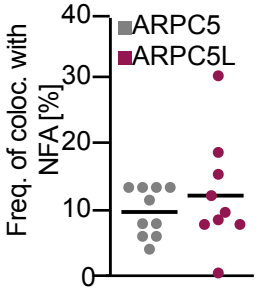

Sadhu et al., 2021: Suppl.Fig.4

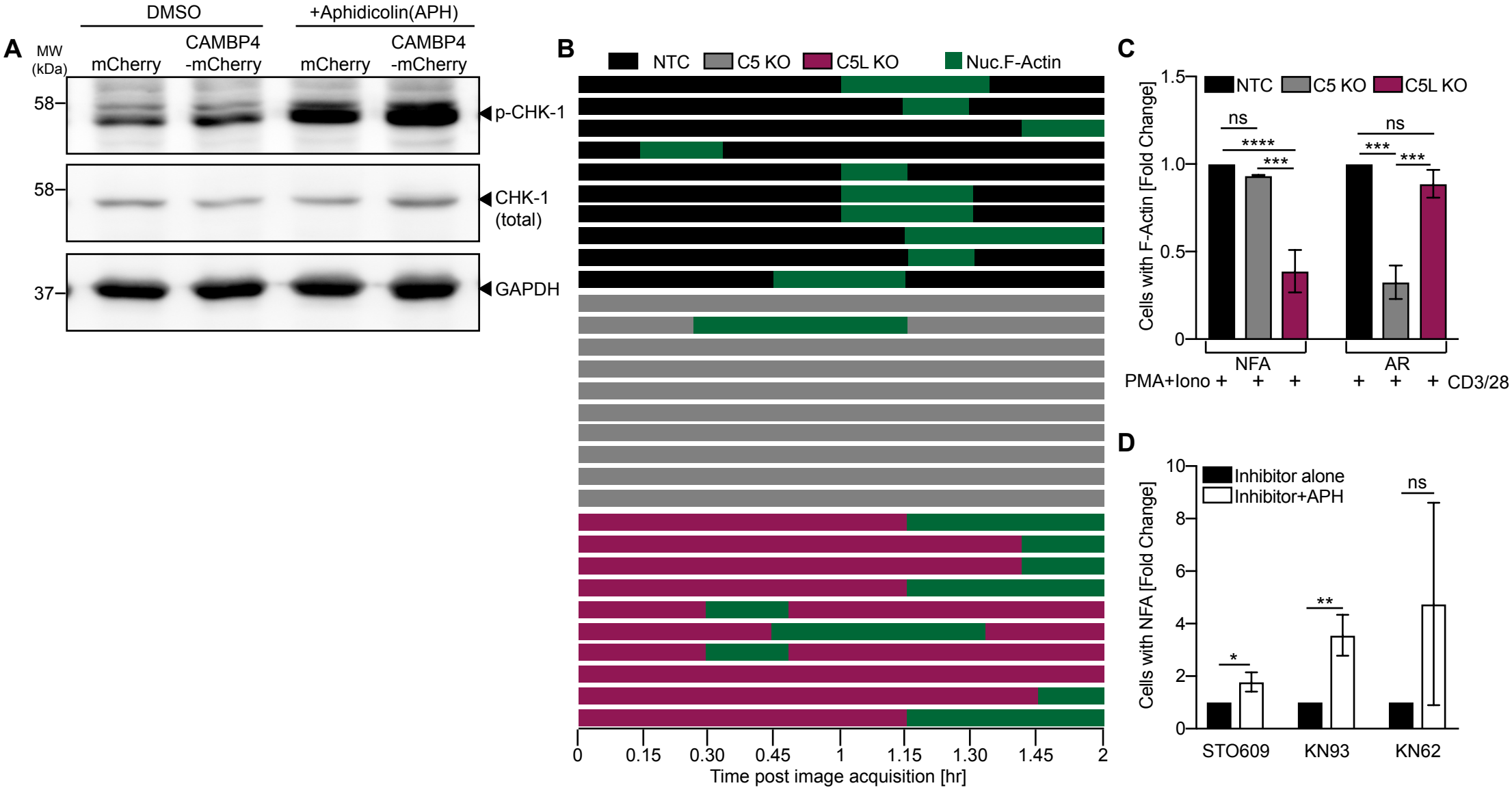

Sadhu et al., 2021: Suppl.Fig.5